# Effect of B-site substitution on the stability of $La_{0.2}Sr_{0.8}Fe_{0.8}B_{0.2}O_{3-\delta}$, B = Al, Ga, Cr, Ti, Ta, Nb

Ørjan Fossmark Lohne[a], Jonas Gurauskis[a], Tan Nhut Phung[b], Mari-Ann Einarsrud[a], Tor Grande[a], Henny Bouwmeester[b], Kjell Wiik[a,*]

[a]*Department of Materials Science and Engineering, Norwegian University of Science and Technology, NO-7491 Trondheim, Norway*
[b]*Inorganic Membranes, Faculty of Science and Technology & MESA+ Institute for Nanotechnology, University of Twente, P.O. Box 217, 7500 AE Enschede, The Netherlands*

**Abstract**

Single phase, cubic perovskites of composition $La_{0.2}Sr_{0.8}Fe_{0.8}B_{0.2}O_{3-\delta}$, B = Al, Ga, Cr, Ti, Ta and Nb, were prepared by spray pyrolysis from aqueous precursor solutions. The effect of B-site substitution on the stability in a $H_2$ containing atmosphere was investigated using temperature programmed reduction (TPR). High temperature X-ray diffraction (HT-XRD) was performed under conditions similar to those in the TPR experiments. $La_{0.2}Sr_{0.8}FeO_{3-\delta}$ forms a brownmillerite-type anion-deficient ordered perovskite upon reduction at $T \approx 500$ °C. B-site substitution suppresses oxygen vacancy ordering, maintaining a perovskite structure under the above reducing conditions up to $T \approx 700$ °C. Trends in the kinetics of decomposition of B-site substituted $La_{0.2}Sr_{0.8}FeO_{3-\delta}$ are discussed.

*Keywords:* MIEC, perovskite, stability, temperature programmed reduction (TPR)

## 1. Introduction

Oxygen permeable dense ceramic membrane technology for production of syn-gas ($H_2$ and CO) from natural gas has been an area of significant research for a number of years [1]. The main challenges, still to overcome, are the development of material systems showing sufficient stability at high temperatures and reducing conditions combined with adequate oxygen transport properties. Teraoka et al. [2] showed perovskite-type oxides $La_{1-x}Sr_xFe_{1-y}Co_yO_{3-\delta}$ to be promising materials for oxygen permeation membranes.By altering the composition with A and/or B-site substitution, both oxygen transport properties and chemical stability may be enhanced [3, 4, 5].

Temperature programmed reduction (TPR) is a fast and efficient method to obtain relative differences of stability in reducing atmospheres for different compositions. Different ex-situ or modeling techniques are used to interpret the different reduction steps throughout the TPR measurements, e.g. X-ray diffraction, $^{57}$Fe Mössbauer spectroscopy and density functional theory (DFT) [4, 6, 7]. In this study we imitate an in-situ characterization through high temperature X-ray diffraction (HT-XRD) to study the structural changes in detail. We investigate the system $La_{0.2}Sr_{0.8}Fe_{0.8}B_{0.2}O_{3-\delta}$ with B = Fe, Al, Ga, Cr, Ti, Ta and Nb, denoted LSF/LSFB, where the transport properties are enhanced by substituting La with the lower valent Sr cation on the A-site, while stability is reinforced by partial substitution of the B-site cation with a reduction-resistant high valent cation.

*Corresponding author
*Email address:* kjell.wiik@material.ntnu.no (Kjell Wiik)

## 2. Experimental

$La_{0.2}Sr_{0.8}Fe_{0.8}B_{0.2}O_{3-\delta}$ (B = Fe, Al, Cr, Ga, Ti, Nb, Ta) powders were made by spray pyrolysis using $Sr(NO_3)_2$ dried at 200 °C for 24 h and aqueous precursor solutions of 0.2 M La-EDTA complex, 0.2 M Ta-peroxo-citrate complex, 0.2 M Nb-peroxo-citrate complex, 0.2 M Ti-isopropoxide-citrate complex, $ZrO(NO_3)_2$ and Fe\Cr\Ga\Al-nitrates. The Ta/Nb-peroxo-citrate complex solutions were prepared following a route based on [8, 9]. Citric acid monohydrate, $C_6H_8O_7 \cdot H_2O$, (3 mol) was dissolved in hydrogen peroxide, $H_2O_2$ (3.6 L, 30 wt%). Ta-oxalate solution or ammonium niobium dioxalate oxide pentahydrate, $(NH_4)NbO(C_2H_4)_2 \cdot 5H_2O$, (1 mol) was added slowly and the solution was heated to $T \approx 60$ °C to start the exothermic decomposition of the oxalate ions. The temperature was controlled with water cooling for safety reasons and the solution was kept at $T \approx 60$ °C until no gas evolution was visible. The pH was adjusted to 6-7 with $NH_4OH$ solution and heated to $T \approx 60$ °C to decompose excess hydrogen peroxide. The solution was once more kept at $T \approx 60$ °C until no gas evolution was visible. The Ti-isopropoxide-citrate complex was synthesized by dissolving citric acid monohydrate, $C_6H_8O_7 \cdot H_2O$, (3 mol) with distilled water (2500 mL) at a temperature of 90 °C. Titanium isopropoxid, $Ti(OCH(CH_3)_2)_4$, (1 mol) was added to the mixture with nitrogen gas flush over the bottle to prevent oxidation to $TiO_2$ (s). The solution was kept on stirring over night at 90 °C until a clear, lemon colored solution was obtained. The details of the La-EDTA complex formation and spray pyrolysis are described elsewhere [10]. As-synthesized powders were calcined at 900 °C for 12 h with subsequent ball milling (YSZ milling balls) in 100% ethanol for 24h. Powders were dried in BUCHI Labortechnik AG

Rotavapor®, mortered, and sieved at 250 µm.

Sample preparation for temperature programmed reduction (TPR) and high temperature X-ray diffraction (HT-XRD) measurements were as follows. Powder samples were uniaxially pressed into cylindrical pellets and sintered at 1300 °C before crushed to $d_p \leq 10$ µm powder by a Retsch MM 2000 mixer mill. The crushed powder was re-annealed at 900 °C for 1 h and cooled at 50 K/h to obtain a homogeneous non-stoichiometry throughout the powder. The TPR measurement was performed by introducing a powder sample of $m_s \approx 100$ mg to a u-tube quartz reactor with a cross section of ⌀3 mm. The sample was pretreated in Ar gas flow at 300 °C for 30 min and cooled to room temperature to remove any volatile species before heating to 1100 °C, with rate of 1 K/min, in a 7% $H_2$/He gas flow of 50 mL/min. The pretreatment and TPR measurement were carried out using a Quantachrome Instruments ChemBET™ TPR/TPD.

X-ray diffraction (XRD) analysis (Bruker D8 Focus with a LynxEye™ detector and Cu-K$\alpha$ radiation) was carried out to check phase purity of the produced powder. High-temperature X-ray diffraction (HT-XRD) analysis (Bruker D8 Advance with a VÅNTEC-I detector, Cu-K$\alpha$ radiation, and mri Physikalische Geräte GmbH Temperature Chamber) was performed to imitate an in-situ XRD analysis of the TPR measurement. Samples were deposited on a heated Pt-Rh strip and the temperature was monitored by an S-type thermocouple placed in contact with the Pt-Rh strip. Measurements were carried out in a 7% $H_2$/He gas mixture. The temperature was incremented stepwise with a heating rate of 1 K/min from room temperature to 1200 °C. XRD scans were recorded isothermally in a period as short as possible to avoid significant interference with the kinetics of reduction.

## 3. Results and discussion

XRD patterns of samples sintered at 1300 °C showed a cubic perovskite with no sign of secondary phases for all compositions.

The TPR profiles of all selected compositions are shown in Fig. 1. All compositions show a narrow peak with onset at ≈ 200 °C before reaching a plateau with a new peak onset at ≈ 700 °C. The first TPR peak can be deconvoluted into a primary and a secondary peak for the compositions LSF, LSFTi, LSFTa and LSFNb. HT-XRD data of LSF in the temperature range 30–600 °C is shown in Fig. 2 (a) and provide evidence for a transition to a brownmillerite-type anion-deficient ordered perovskite structure, $(Sr,La)_3Fe_3O_8$ [11], at $T \approx 350$ °C. Hence, for LSF the process of ordering the oxygen vacancies is considered to be responsible for the splitting of the first TPR peak. Oxygen vacancy ordering is detrimental to the ionic transport properties of perovskites, and a brownmillerite type structure is therefore not desired in materials for membrane applications. HT-XRD of LSFTa in the temperature range 30-700 °C, Fig. 2 (b), demonstrate no such transition and the perovskite structure is stable at $T < 700$ °C. The peak shift around 200 °C is due to chemical expansion assigned to the change in unit cell parameters from the reduction of $Fe^{4+}$ to $Fe^{3+}$. For the sake

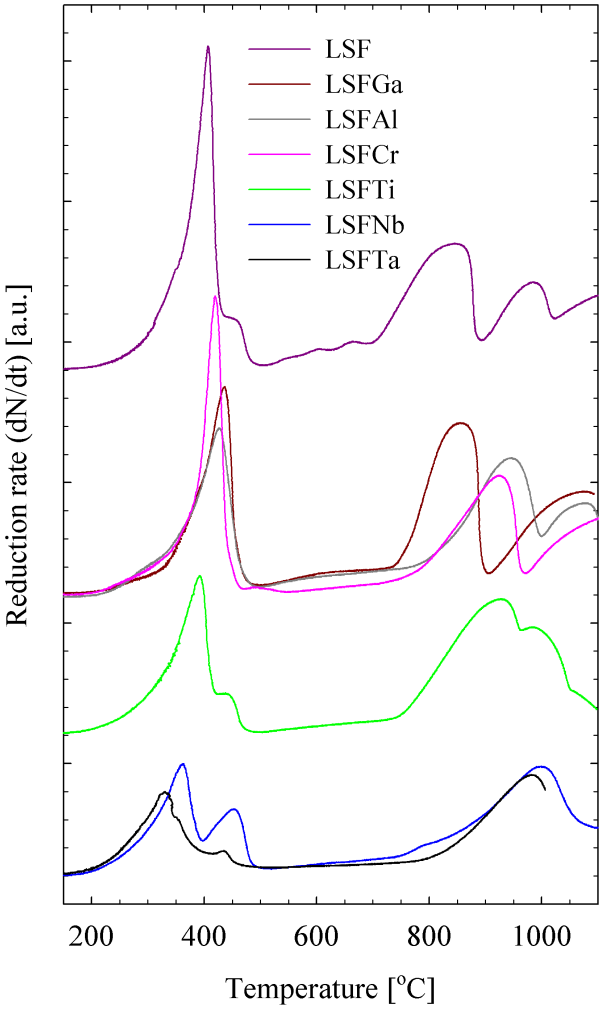


Fig. 1. TPR profile of $La_{0.2}Sr_{0.8}Fe_{0.8}B_{0.2}O_{3-\delta}$. Heating rate 1 K/min.

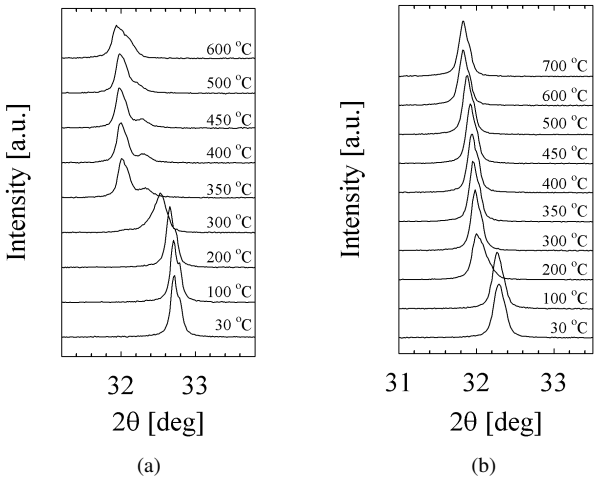


Fig. 2. HT-XRD at low temperatures of (a) $La_{0.2}Sr_{0.8}FeO_{3-\delta}$ and (b) $La_{0.2}Sr_{0.8}Fe_{0.8}Ta_{0.2}O_{3-\delta}$

of clarity, only the main peaks have been included in Fig. 2. The remaining peaks have all been identified and matched to the phases mentioned. Although not included here, HT-XRD was additionally performed on LSFAl and LSFTi where both perovskite structures remained stable at $T < 700$ °C. Hence, B-site substitution of $La_{0.2}Sr_{0.8}FeO_{3-\delta}$ suppresses the formation of the anion-deficient ordered perovskite structure, $(Sr,La)_3Fe_3O_8$. Since there are no structural changes, apart from a change in the lattice constants due to chemical expansion, the secondary TPR peak observed for compositions LSFTi, LSFTa and LSFNb is assigned to a difference in the local environment of the oxygen anions, associated with the higher Coulombic fields of the dopant cations relative to that of the parent cations.

HTXRD of LSF around the next reduction step at $T \approx 700$ °C, Fig. 3 (a), reveal a decomposition to a Ruddlesden-Popper phase, $La_{2-x}Sr_xFeO_4$ [12], and the first traces of metallic Fe(s), similar to what reported by Berry et.al.[4]. The full decomposition of LSF into Fe(s), $La_2O_3$ [13] and SrO [14] starts at $T \approx 900$ °C and accounts for the remaining TPR-peaks. The unidentified XRD peak at $\approx 43°$ is due to a reaction between Fe(s) and the Pt-Rh strip at high temperatures. HT-XRD of LSFTa, Fig. 3 (b), show the same steps as for LSF where the reduction at $T \approx 700$ °C is a decomposition to a RP-type phase and the following step is the decomposition into Fe(s), La2O3, SrO and $Sr_3TaO_{5.5}$ [15]. The decomposition of the perovskite is apparent for all compositions within a small temperature range and it is obvious that B-site substitution does not significantly change the thermodynamic stability of the LSF perovskite structure. There seems, however, to be a kinetic stabilization of the lattice obtained by B-site substitution. To get an overview of the change in stability between compositions we focus on the TPR peak at $T \approx 700$ °C since this is the first step of decomposition of the perovskite. Both the onset and peak temperature are shown in Fig. 4. LSF has both the lowest onset and peak temperature, and thus all the different B-substituted ions improve the apparent stability of the material. The ionic radii of $Ta^{5+}$ and $Nb^{5+}$ are very close to that of $Fe^{3+}$ [16], and the effect of high valent substitution is clearly visible. LSFAl, LSFCr and LSFGa, however, demonstrate quite different results relative to each other even though their valencies are the same. The main difference between these three cations is their ionic size. Ionic radii for the different cations are shown in Tab. 1. Comparing the data presented in Tab. 1 and Fig. 4 one sees that the trend for the different $B^{3+}$ dopant cations is that of an increased stability with decreasing size. This is also supported by considerations of the Goldschmidt tolerance factor, $t$ [17], which approaches unity (ideal perovskite) as the B-site cation is substituted with a smaller cation. Hence, the kinetic stabilization of B-site substituted LSF is both an effect of the valence and the size of the B dopant. Although the differences in onset temperatures discussed here are within a narrow temperature region, decreasing the heating rate of the TPR-measurement will further increase the temperature difference between samples. This kinetic stabilization, although seemingly small, might be sufficient to prevent decomposition of the membrane taking into consideration that these materials, used as oxygen separation membranes, will be operated at steady-state conditions. Given

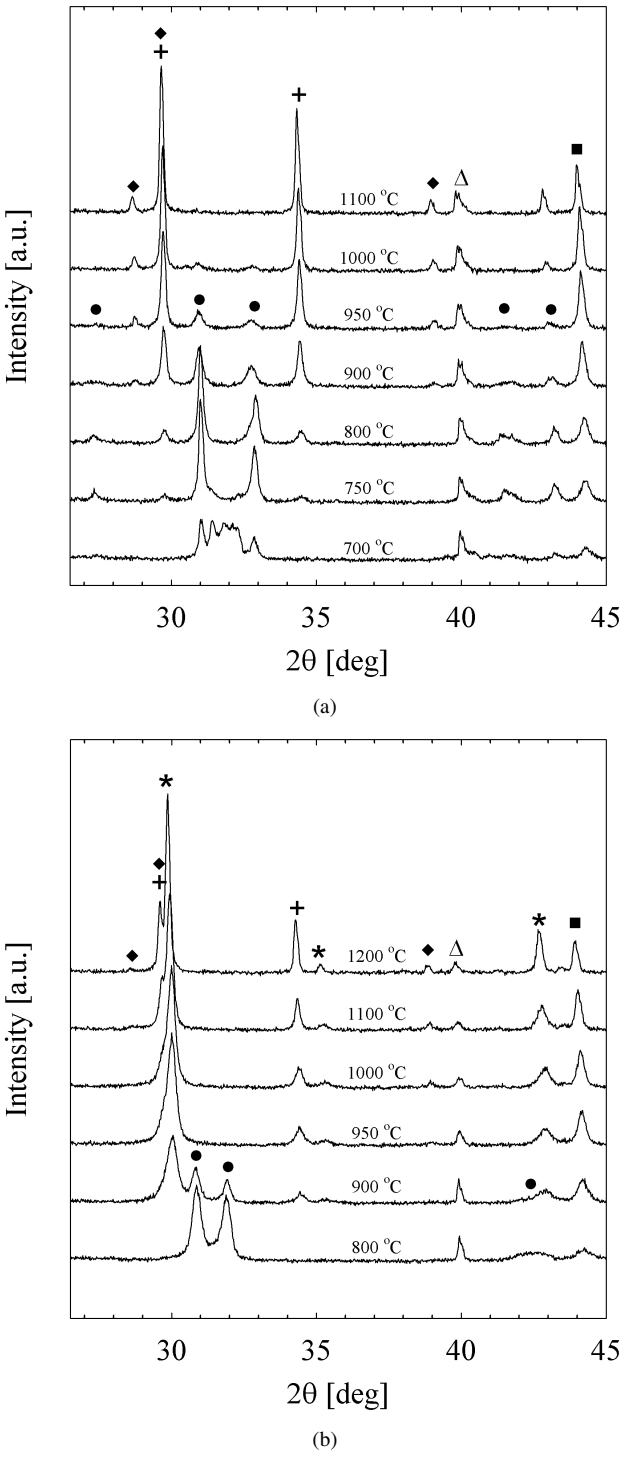


Fig. 3. HT-XRD at high temperatures of (a) $La_{0.2}Sr_{0.8}FeO_{3-\delta}$ and (b) $La_{0.2}Sr_{0.8}Fe_{0.8}Ta_{0.2}O_{3-\delta}$. Phases identified as ♦ $La_2O_3$, + SrO, Δ Pt, ■ Fe, • $La_{2-x}Sr_xFeO_4$-type, ∗ $Sr_3TaO_{5.5}$

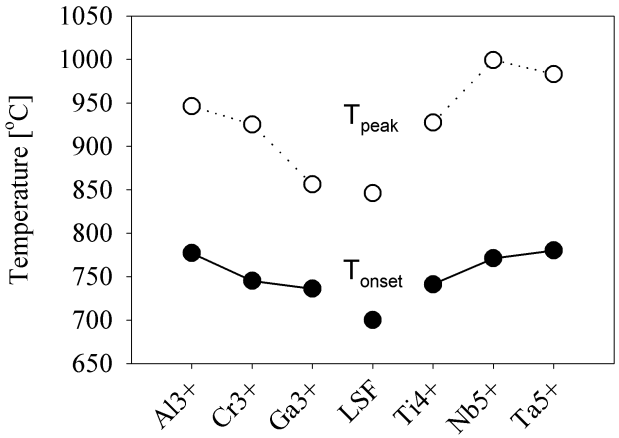


Fig. 4. Onset temperatures (closed circles) and peak temperatures (open circles) of the TPR peak at $T \approx 700$ °C for LSFB. Lines are added as guide to the eye

that the oxygen permeation flux is controlled by surface exchange on the fuel side (reducing conditions), the oxygen activity at the surface might be sufficiently high to suppress decomposition of the perovskite. Oxygen permeation measurements of LSFTa asymmetric dense membranes on porous support have been performed [18] and long-term stability measurements in reducing and reactive atmospheres are being carried out and will be reported elsewhere.

Table 1. Ionic radii of different cations [16]

| $B^{n+}$ | *Ionic radius [Å]* |
|---|---|
| $Al^{3+}$ | 0.535 |
| $Fe^{4+}$ | 0.585 |
| $Ti^{4+}$ | 0.605 |
| $Cr^{3+}$ | 0.615 |
| $Ga^{3+}$ | 0.620 |
| $Ta^{5+}$ | 0.64 |
| $Nb^{5+}$ | 0.64 |
| $Fe^{3+}$(HS) | 0.645 |

## 4. Conclusions

B-site substitution of $La_{0.2}Sr_{0.8}FeO_{3-\delta}$ suppresses the formation of a brownmillerite-type phase at low temperatures at reducing conditions (7% $H_2$ \ 93% Ar). The first step of decomposition of the perovskite, in a $H_2$ containing atmosphere, is to a Ruddlesden-Popper, $K_2NiO_4$-type of structure with the excess Fe reduced to Fe(s). Analysis of TPR data reveals that the onset temperature of this decomposition has increased for all B-substituted compositions relative to that of the parent undoped material. Among the different compositions, LSFAl, LSFTa and LSFNb shows the highest apparent stability with the highest onset temperatures for decomposition in the TPR experiments. The increase in apparent stability is a kinetic effect. $Al^{3+}$ substitution increased the stability due to a size effect from the low ionic radius of $Al^{3+}$ compared to $Fe^{3+}$(HS), while $Nb^{5+}$ and $Ta^{5+}$ substituted samples possess a higher stability due to the increased electrostatic forces from the high valence of these ions. None of the compositions is thermodynamically stable at the conditions applied here, but taking into consideration that the difference between samples is a kinetic effect and the application is as oxygen separation membranes, decomposition of the perovskite may be suppressed at the fuel side.

## Acknowledgment

Funding provided by the Norwegian Research Council (NFR), FRINAT-project no. 191358: The kinetics of surface exchange reactions in oxide based mixed conductors at reducing conditions and high temperatures, is acknowledged.

## References

[1] H. J. M. Bouwmeester, Catalysis Today 82 (2003) 141–150.
[2] Y. Teraoka, H. M. Zhang, S. Furukawa, N. Yamazoe, Chemistry Letters (1985) 1743–1746.
[3] Y. Teraoka, T. Nobunaga, N. Yamazoe, Chemistry Letters (1988) 503–506.
[4] F. J. Berry, J. F. Marco, X. Ren, Journal of Solid State Chemistry 178 (2005) 961–969.
[5] S. Diethelm, D. Bayraktar, T. Graule, P. Holtappels, J. Van herle, Solid State Ionics 180 (2009) 857–860.
[6] S. Ivanova, A. Senyshyn, E. Zhecheva, K. Tenchev, R. Stoyanova, H. Fuess, Journal of Solid State Chemistry 183 (2010) 940–950.
[7] L. M. Petkovic, V. Utgikar, S. N. Rashkeev, Journal of Physical Chemistry C 115 (2011) 8709–8715.
[8] Y. Narendar, G. L. Messing, Chemistry of Materials 9 (1997) 580–587.
[9] D. Nelis, K. Van Werde, D. Mondelaers, G. Vanhoyland, M. K. Van Bael, J. Mullens, L. C. Van Poucke, Journal of the European Ceramic Society 21 (2001) 2047–2049.
[10] T. Mokkelbost, Ø. Andersen, R. A. Strøm, K. Wiik, T. Grande, M. A. Einarsrud, Journal of the American Ceramic Society 90 (2007) 3395–3400.
[11] P. D. Battle, T. C. Gibb, P. Lightfoot, Journal of Solid State Chemistry 84 (1990) 237–244.
[12] J. L. Soubeyroux, P. Courbin, L. Fournes, D. Fruchart, G. Le Flem, Journal of Solid State Chemistry 31 (1980) 313–320.
[13] H. Müller-Buschbaum, H. G. V. Schnering, Zeitschrift für anorganische und allgemeine Chemie 340 (1965) 232–245.
[14] B. J. Reardon, C. R. Hubbard, Powder diffraction 7 (1992) 96–98.
[15] L. H. Brixner, Journal of the American Chemical Society 80 (1958) 3214–3215.
[16] R. D. Shannon, Acta Crystallographica Section A 32 (1976) 751–767.
[17] V. M. Goldschmidt, T. Barth, G. Lunde, W. Zachariasen, Geochemische verteilungsgesetze der elemente, Pt. VII Skrifter, Det Norske videnskabs-akademi, Oslo, 1926.
[18] J. Gurauskis, Ø. F. Lohne, K. Wiik, Solid State Ionics In press – This issue (2011).